

Research Paper

Development of Sialic Acid-coated Nanoparticles for Targeting Cancer and Efficient Evasion of the Immune System

Young-Hwa Kim^{1*}, Kyung Hyun Min^{1*}, Zhantong Wang¹, Jihoon Kim¹, Orit Jacobson¹, Peng Huang², Guizhi Zhu¹, Yijing Liu¹, Bryant Yung¹, Gang Niu¹, and Xiaoyuan Chen¹

1. Laboratory of Molecular Imaging and Nanomedicine, National Institute of Biomedical Imaging and Bioengineering, National Institutes of Health, Bethesda, Maryland 20892, United States.
2. Guangdong Key Laboratory for Biomedical Measurements and Ultrasound Imaging, School of Biomedical Engineering, Shenzhen University, Shenzhen 518060, P. R. China.

*These authors contributed equally to this work.

 Corresponding authors: **Dr. Xiaoyuan Chen**, Laboratory of Molecular Imaging and Nanomedicine, National Institute of Biomedical Imaging and Bioengineering, National Institutes of Health, Bethesda, Maryland 20892, United States. E-mail: shawn.chen@nih.gov. **Dr. Gang Niu**, Laboratory of Molecular Imaging and Nanomedicine, National Institute of Biomedical Imaging and Bioengineering, National Institutes of Health, Bethesda, Maryland 20892, United States. Email: Gang.Niu@nih.gov.

© Ivyspring International Publisher. This is an open access article distributed under the terms of the Creative Commons Attribution (CC BY-NC) license (<https://creativecommons.org/licenses/by-nc/4.0/>). See <http://ivyspring.com/terms> for full terms and conditions.

Received: 2017.01.05; Accepted: 2017.01.14; Published: 2017.02.23

Abstract

Evading the reticuloendothelial system (RES) remains a critical challenge in the development of efficient delivery and diagnostic systems for cancer. Sialic acid (N-acetylneuraminic acid, Neu5Ac) is recognized as a “self” marker by major serum protein complement factor H and shows reduced interaction with the innate immune system *via* sialic acid-binding immunoglobulin-like lectin (Siglec), which is known as one of the significant regulators of phagocytic evasion. Accordingly, we prepared different surface-modified gold nanoparticles (AuNPs) and investigated the effects of sialic acid on cellular and immune responses of nanoparticles *in vitro* and *in vivo*. Sialic acid modification not only facilitates evasion of the RES by suppressing the immune response, but also enhances tumor accumulation *via* its active targeting ability. Therefore, sialic acid modification presents a promising strategy to advance nanotechnology towards the prospect of clinical translation.

Key words: sialic acid (N-acetylneuraminic acid, Neu5Ac), anti-recognition effect, evading phagocytosis, lectin targeting, molecular imaging, positron emission tomography (PET).

Introduction

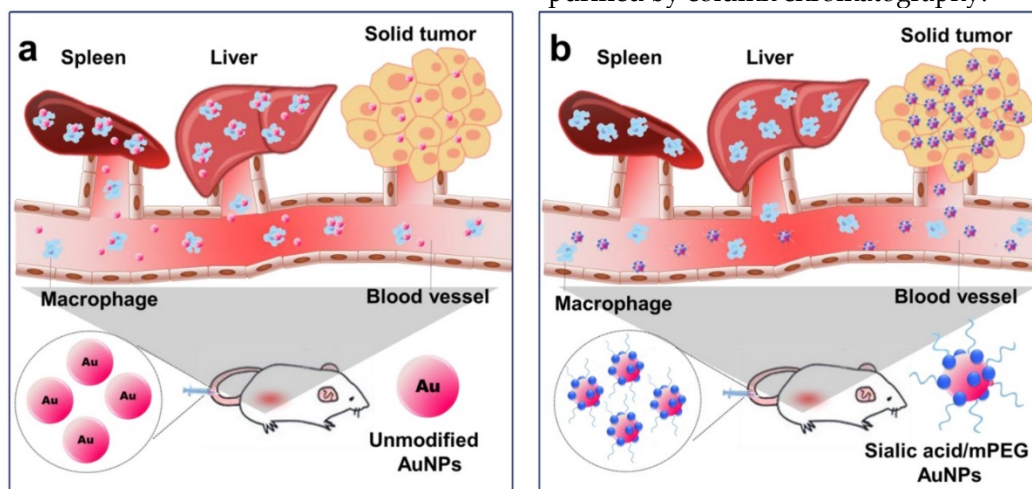
The immune system mediated clearance of nanoparticles remains a significant challenge for clinical application despite their promising potential in site specific accumulation *via* passive or active targeting [1-4]. Accordingly, there have been tremendous efforts to prevent nanoparticles from being uptaken by the reticuloendothelial system (RES) by means of red blood cell (RBC) membrane biomimetics, CD47, polyethylene glycol (PEG), *etc.* [5, 6]. Among these, PEG is the most widely used material to reduce uptake by the mononuclear phagocyte system (MPS) for improving the stealth effect because of its low cost and ease of modification

[7-9]. However, PEGylated nanoparticles have a potential drawback in diagnostic and therapeutic efficacy due to the production of PEG-specific antibodies [10-13]. In addition, PEG coating onto nanoparticles has been reported to mitigate the drug release and target cell interaction, thus compromising the diagnostic and therapeutic goals [14, 15]. Therefore, there is an unmet need for developing new strategies capable of enhancing the stealth effect or substituting the effects of PEG.

One of the significant regulators of evading phagocytosis is sialic acid (N-acetylneuraminic acid, Neu5Ac), an acidic nine-carbon sugar that binds to

immunosuppressive carbohydrate-recognition receptors, notably sialic acid-binding immunoglobulin-like lectin (Siglec) expressed by immune cells [16, 17]. Sialic acid is capable of regulating the alternative pathway of complement activation. Major serum protein complement factor H recognizes sialic acid as a “self” marker, which helps to inhibit C1q/C3b fragment activation [18-22]. Siglec, which is broadly expressed in the innate immune system, has an intracellular immunoreceptor tyrosine-based inhibition motif (ITIM) that can mediate inhibitory signals upon binding to sialic acid and activate downstream inhibitory signaling through the recruitment of tyrosine phosphatases SHP-1 and SHP-2 [23-27]. In addition, sialic acid can also be used as a targeting ligand owing to its specific binding to a carbohydrate-binding lectin overexpressed in several types of cancers [28-30]. Sialic acid-covered nanoparticles are expected to facilitate inhibition of immune cell activation, which allows RES escape by rendering the nanoparticles prolonged circulation in the blood stream and reduced uptake by the immune system. It is also expected that sialic acid-covered nanoparticles can target more specifically to the tumor site by maximizing the benefit of nanoparticles *via* multivalent high avidity binding of sialic acid to lectin [31, 32].

Herein, we compare the effects of sialic acid as well as different charged PEGylated nanoparticles in phagocytosis and immune activation. The results suggest that modification of nanoparticles with sialic acid results in decreased clearance by the MPS and improve their effectiveness as targeting moieties *in vitro* and *in vivo* (Scheme 1).



Scheme 1. Illustration of AuNP distribution and tumor targeting (a) Unmodified AuNPs are phagocytized by the reticuloendothelial system (RES) and only a small amount of AuNPs are delivered to tumor cells. (b) Sialic acid-mPEG-AuNPs can escape RES uptake and efficiently target tumor cells.

Materials and Methods

Remarks and materials

Chemical structures, synthesis schemes, and detailed experimental methods are described in the Supporting Information section. All animal experiments were conducted in accordance with an approved NIH protocol.

General methods

Cells were purchased from the American Type Culture Collection (Rockville, MD, USA). Other chemicals and biological materials were purchased from Sigma-Aldrich Co. (St. Louis, MO, USA) or Invitrogen (Carlsbad, CA, USA) unless otherwise noted and used without further purification.

Synthesis of 20 nm gold nanoparticles

To synthesize 20 nm gold nanoparticles, 10 mg HAuCl_4 was dissolved in 100 mL H_2O and heated to boiling under constant stirring. Then sodium citrate solution (1.8 mL, 1 wt%) was quickly injected. The whole solution was kept at 100°C for 30 min and then cooled down to room temperature. The 20 nm gold nanoparticles were stored at 4°C for further use.

Synthesis of N-acetyl-6-S-acetyl-6-thiomannosamine

To improve solubility for N-Acetylneuraminic acid (Neu5Ac), the free acid form was converted into the triethylammonium salt. A solution of N-Acetylneuraminic triethylammonium salt (212 mg, 0.50 mmol) and thioacetic acid (0.14 mL, 1.97 mmol) in dry DMF (3.0 mL) was added at 0°C to a solution of TPP (236 mg, 0.90 mmol) and DEAD (0.14 mL, 0.90 mmol) in THF (2.5 mL). The reaction mixture was allowed to acclimate to room temperature and was stirred for 3 h. The reaction product was further purified by column chromatography.

Synthesis of N-acetyl-9-thioneuraminic acid

1 N NaOMe in MeOH (0.5 mL) was added to a solution of N-acetyl-6-S-acetyl-6-thiomannosamine (100 mg, 0.272 mmol) in MeOH (8 mL) at 0°C. The mixture was stirred for 2 h, then neutralized with Amberlite IR 120 (H⁺) and filtered. After addition of water (3 mL), the solution was concentrated under vacuum to ~ 0.5 mL and passed at 4°C through a column of Amberlite IR 120 (H⁺). Residual solvent was removed by freeze drying to yield N-acetyl-9-thioneuraminic acid.

Characterization of AuNPs

The zeta potential and size of the gold nanoparticles were measured by a nanoparticle analyzer (SZ-100, HORIBA, Kyoto, Japan). Transmission electron microscopy (TEM) was used to observe the particle size and morphology of AuNPs (JEM 2010, Jeol Ltd, Tokyo, Japan). The UV-Vis absorption spectra were measured with a Genesys 10S UV-vis spectrophotometer (Thermo Fisher Scientific, Waltham, MA, USA).

Cell culture and animals

The murine macrophage cell line RAW264.7 and murine breast cancer cell line 4T1 were obtained from the American Type Culture Collection (ATCC, Rockville, MD, USA) and were maintained in Dulbecco's Modified Eagle Medium (DMEM) and RPMI 1640, respectively, with further supplemented 10% fetal bovine serum, 100 U/mL penicillin, and 100 µg/mL streptomycin (Gibco, Grand Island, NY, USA). Cells were grown to confluency at 37°C in a humidified atmosphere containing 5% CO₂. Mice were inoculated subcutaneously with 1 × 10⁶ of 4T1 cells on the right flank of 6-7 week old FVB mice (n = 4/group). When the tumors reached an approximate volume of 500 mm³, PET imaging studies were completed. Tumor growth was monitored by caliper measurement. All animal experiments were performed under a National Institutes of Health Animal Care and Use Committee (NIHACUC) approved protocol.

Cytotoxicity assay

The murine macrophage RAW264.7 cells were cultured in 96-well plates at a density of 1 × 10⁴ cells/well. Different concentrations of AuNPs (0.8 ~ 200 µg/mL) were added into each well and the mixture was incubated at 37°C for 24 h and 48 h. After incubation, PBS was used to wash the cells twice. AlamarBlue® reagent (Thermo Fisher Scientific, Waltham, MA, USA) was added as 10% of the sample volume to each well and the plate was incubated at 37°C for another 3 h. The absorbance was measured

by a plate reader at 570 nm, and the cell viability was calculated. Cell viabilities were normalized untreated control group.

In vitro darkfield microscopy imaging

Darkfield images were taken with a Zeiss Axioskop 2 plus microscope equipped with a black-white CCD camera. All images were taken at 60X magnification under the same lighting conditions using an Olympus IX-81 inverted epifluorescence microscope (Olympus, Tokyo, Japan).

Inductively coupled plasma mass spectroscopy (ICP-MS)

Quantification of AuNPs was performed using ICP-MS. RAW264.7 cells were seeded onto a 6-well plate, and one day later, the cells were treated with each AuNP formulation (15 µg/mL) for 24 h, respectively. Cells of interest were harvested and digested in a mixture of HNO₃ (50 µL ~25 %) and HCl (150 µL ~75 %). 50 µL of AuNPs were also digested in a mixture of HNO₃ (25 µL ~25 %) and HCl (75 µL ~75 %). The samples digested in 2~3% w/v HNO₃ were diluted with ultrapure water to 5 mL. Both sample preparations were performed on the same day of the measurements. The total elemental concentrations of the samples were determined by means of ICP-OES (Agilent 700 Series ICP Optical Emission Spectrometers, Santa Clara, CA, USA).

RT-PCR analysis

The total RNA content was isolated from AuNP treated RAW264.7 cells using TRIzol reagent (Invitrogen, Grand Island, NY, USA) according to manufacturer's instruction, and then RNA quantity was assessed using a Nanodrop spectrophotometer (Thermo Fisher Scientific, Waltham, MA, USA). For PCR, cDNA was synthesized from total RNA using Verso cDNA synthesis Kit (Thermo Fisher Scientific, Waltham, MA, USA). The sequences of the forward and reverse primers of CD14 were 5'-ACTTTCAAGGCCAGGAGTG and 5'-AGGTG GGACCACAGAGAGTT, respectively. The sequences of the forward and reverse primers of CD86 were 5'-GCGGGATAGTAACGCTGACA and 5'-ACCACT CCCATCCTGACTGA, respectively. The sequences of the forward and reverse primers of F4/80 were 5'-ACTTTCAAGGCCAGGAGTG and 5'-AGGTG GGACCACAGAGAGTT, respectively. The sequences of the forward and reverse primers of β-actin were 5'-TGAGCTGCGTTTTACACCCT and 5'-AGGGTG AGGGACTTCCGTGTA, respectively. The PCR reaction (94°C for 30 s, 60°C for 30 s, 72°C for 30 s) was run for 30 cycles after an initial single cycle of 94°C for 2 min to activate the Taq polymerase. After 30 cycles of amplification, PCR products were analyzed by gel

electrophoresis in 1.5% agarose gels and visualized by GelRed™ (Biotium, Hayward, CA, USA) staining. The results were analyzed by one-way ANOVA with Newman-Keuls Multiple Comparison test using Prism software (GraphPad Software Inc., La Jolla, CA, USA) to determine if differences between groups were statistically significant ($p < 0.05$).

In vitro confocal microscopy imaging

For confocal imaging, macrophages were plated in coverslip-bottom culture chambers (LabTEK) to confluency and fixed in 1x PBS with 4% w/v paraformaldehyde for 30 min at room temperature. The cells were then washed with PBS three times and incubated with anti-CD14-FITC, anti-CD86-FITC, anti-F4/80-PE, or anti-CD301-APC (BD Pharmingen™, San Diego, CA, USA) for 1 h at room temperature, respectively. Cells were then washed with PBS three times and mounted with antifade mounting medium with DAPI (Vectashield, Burlingame, CA, USA). Confocal microscopy was then performed with an Olympus Fluoview FV10i automated confocal laser-scanning microscope (Olympus, Tokyo, Japan).

In vitro immunoactivation

In vitro immunoactivation was characterized using flow cytometry and enzyme-linked immunosorbent assay (ELISA). Flow cytometry was used to study the expression levels of costimulatory markers and maturation markers. Specifically, RAW264.7 cells were seeded into a 6-well plate, and one day later, the cells were treated with each AuNP formulation (15 $\mu\text{g}/\text{mL}$) for 24 h. Cells of interest were harvested and stained for 30 min at 4°C with anti-CD14-FITC, anti-CD86-FITC, or anti-F4/80-PE targeting plasma surface markers. Then the cells were washed and resuspended in FACS buffer. All flow cytometry analyses were performed on a BD Accuri C6 (BD Bioscience, San Jose, CA, USA) and data were analyzed by Flowjo (TreeStar, Ashland OR, USA). Alternatively, enzyme-linked immunosorbent assay (ELISA) was used to measure the concentration of secreted proinflammatory cytokines by immune cells upon immunoactivation. RAW264.7 cells were treated with each AuNP formulation (15 $\mu\text{g}/\text{mL}$) for 24 h. The cell culture medium was then collected and centrifuged to remove any debris. The concentrations of cytokines (e.g., TNF- α and IL-6) in the culture medium of RAW264.7 cells were assayed using ELISA (R&D Systems, Minneapolis, MN, USA) per the manufacturer's instructions. The results were analyzed by one-way ANOVA with Newman-Keuls Multiple Comparison test using Prism software (GraphPad Software Inc., La Jolla, CA, USA) to determine if differences between groups were

statistically significant ($p < 0.05$).

⁶⁴Cu labeling of AuNPs

To prepare radioactive [⁶⁴Cu]-labeled AuNPs, 4 μL of ⁶⁴CuCl₂ was premixed with 1.2 mg of Na-ascorbate (in 0.1 M borate buffer pH 8.6). Then 100 μL of unmodified AuNPs, COOH-PEG AuNPs, NH₂-PEG AuNPs, mPEG AuNPs, and sialic acid/mPEG AuNPs (2 mg/mL) was added, respectively. The mixture was incubated at 37°C for 1 h. The resulting [⁶⁴Cu]-labeled AuNPs were purified by centrifugation (4000 g, 5 min) three times to remove the unreacted [⁶⁴Cu] and excess amount of reagents. The purified [⁶⁴Cu]-labeled AuNPs were finally dispersed in PBS. The labeling efficiency was determined by using instant thin-layer chromatography (ITLC) plates and 0.1 M citric acid (pH 5) as an eluent.

MicroPET imaging and biodistribution

4T1 tumor bearing mice were injected through the tail vein with 50 μCi of ⁶⁴Cu-AuNPs in saline. MicroPET/X-ray imaging experiments were conducted on a Genesys4 PET scanner (Sofie Biosciences, Culver City, CA, USA). 5-10 min static microPET images were acquired under general anesthesia (isoflurane/O₂) at 1 h, 4 h, 24 h and 48 h post-injection. Image data was automatically reconstructed using a 3D MLEM algorithm, which was evaluated by ROI analysis with the AMIDE software package. ROIs were drawn in the tumor, heart, liver, and spleen with results expressed as % ID/cm³ of tissue. After 50 h, mice were sacrificed and blood and major organs were harvested, weighed, and assayed with a gamma counter (Wallac Wizard 1480, PerkinElmer, Waltham, MA, USA) for biodistribution studies. Radioactivity associated with each organ was expressed as a percentage of injected dose per gram of tissue (%ID/g) for a group of 4 animals.

Ex vivo histological staining

4T1 tumor-bearing mice were sacrificed 50 h after AuNP injection. Tumors and major organs were collected, fixed in Z-Fix solution (Anatech Ltd., Battle Creek, MI), and stored at room temperature. Hematoxylin and eosin (H&E) staining slides were prepared by Histoserv (Germantown, MD, USA) and observed using a BX41 bright field microscope (Olympus, Tokyo, Japan).

Statistical analysis

At least three independent samples were tested in each group, and data were expressed as mean \pm SD with statistical significance determined using one-way ANOVA (and nonparametric). ANOVA was

used for multiple comparisons (GraphPad Software Inc., La Jolla, CA, USA). $p < 0.05$ was considered as statistically significant.

Results and Discussion

Preparation and characterization of AuNPs

In this study, gold nanoparticles (AuNPs) were employed as a model system to investigate the potential of sialic acid coating to yield immunologically inert nanoparticles with good biocompatibility, simple synthesis, controllable size, and large surface-to-volume ratio [33-35]. In particular, the thiol-mediated place-exchange reaction allows simple functionalization of the surface of AuNPs [36].

Prior to the preparation of sialic acid modified AuNPs, thiolated sialic acid was synthesized *via* a two-step reaction [37]. Briefly, sialic acid was reacted with thioacetic acid (AcSH) under Mitsunobu condition, and the resultant *S*-acetyl group was converted to a thiol group *via* *S*-deacetylation using methanolic methoxide (Figure S1). In $^1\text{H-NMR}$, up-shifted protons of H-9 and H-9' at 2.9 and 2.7 ppm respectively were observed compared to the parent

sialic acid (Figure S2). In addition, the mass peak at 324 m/z was attributed to the $[\text{M-H}]^-$ of thiolated sialic acid (Figure S3). These results demonstrate the successful synthesis of thiolated sialic acid.

The resultant thiolated sialic acid was mixed with citrate-stabilized AuNPs (~20 nm) and then methoxy polyethylene glycol (mPEG) to yield sialic acid/mPEG AuNPs. mPEG modified AuNPs (mPEG AuNPs) were used as a control and negatively and positively charged PEGylated AuNPs, COOH-PEG AuNPs and NH_2 -PEG AuNPs respectively, were prepared to investigate whether surface charge modulates the immune response. After surface modification, the morphology was retained (Figure 1a) and the UV-vis absorbance was not changed after surface modification, indicating that AuNPs have enough colloidal stability to prevent self-aggregation (Figure 1b). The hydrodynamic size of nanoparticles was increased due to the hydrophilic shell formed by PEG (Figure 1c) and the surface charge of each PEG modified AuNP was in accordance with the corresponding functional end groups of each PEG (Figure 1d). The slightly negative charge of sialic acid/mPEG AuNPs was attributed to the carboxylic

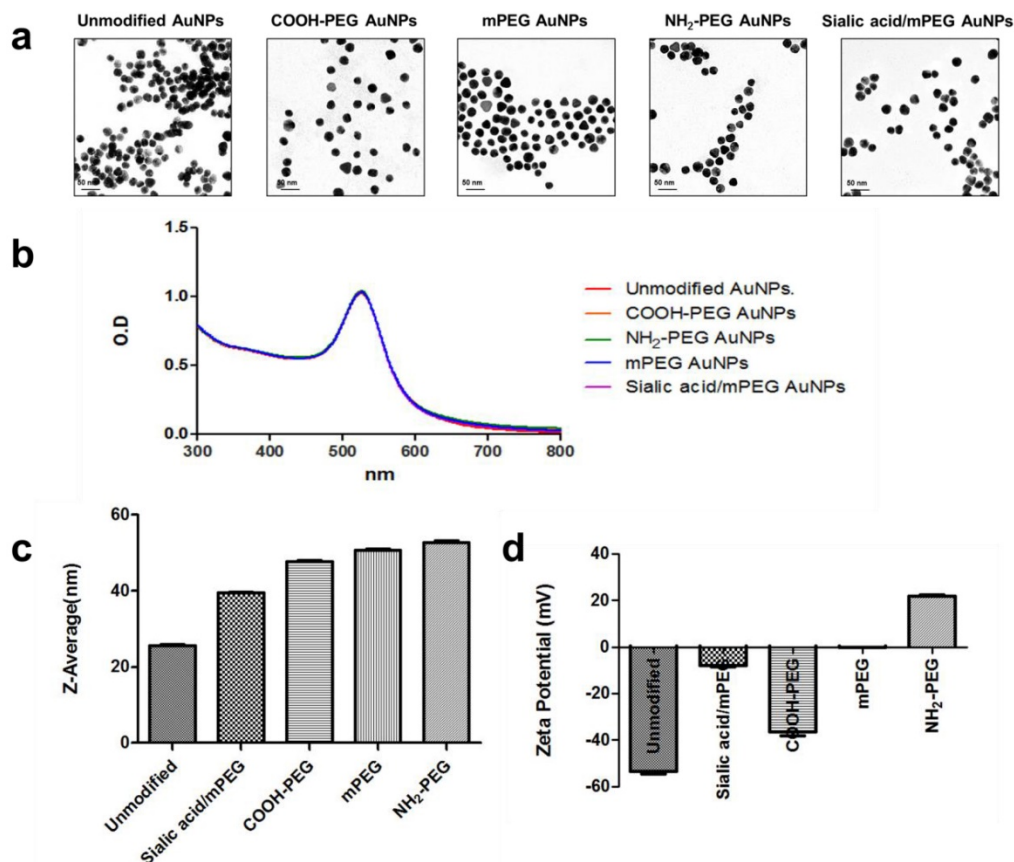


Figure 1. Characterization of AuNPs. (a) Representative TEM images of five different kinds of AuNPs. (b) UV-vis absorbance spectra of five different kinds of AuNPs with or without surface modification. (c) Average size distribution (nm) of five different kinds of AuNPs as measured by DLS (n=5). (d) The zeta potential values (mV) of five different kinds of AuNPs (n=5).

acid group of sialic acid [38]. The size and zeta potential of AuNPs are summarized in Table S1.

Reduced cellular uptake by sialic acid *in vitro*

We presumed that the modification by sialic acid facilitates the evasion of phagocytosis of nanoparticles by macrophages (Figure 2a). To confirm our assumption, cellular uptake of each type of AuNP by murine macrophage cell line RAW264.7 was evaluated *in vitro* using darkfield microscopy (Figure 2b). All AuNPs showed insignificant cytotoxicity up to $200 \mu\text{g mL}^{-1}$, owing to the biocompatibility of AuNPs and PEG (Figure S4). The citrate-capped unmodified AuNPs showed high cellular uptake, which was attributed to the nonspecific adsorption of serum proteins that may contribute to

receptor-mediated endocytosis [39]. As expected, the modification of PEG and sialic acid exhibited reduced cellular uptake as compared with unmodified AuNPs. To confirm the effects of surface charge as well as sialic acid in cellular uptake quantitatively, the intracellular Au content was measured by inductively coupled plasma mass spectroscopy (ICP-MS) (Figure 2c). Positively charged NH_2 -PEG AuNPs showed higher cellular uptake than negatively charged COOH-PEG AuNPs and neutral mPEG AuNPs, in accordance with previous reports [40]. In particular, the sialic acid/mPEG AuNPs exhibited two-fold lower cellular uptake than mPEG AuNPs, evidencing the stealth effect of sialic acid in evading phagocytosis by macrophages.

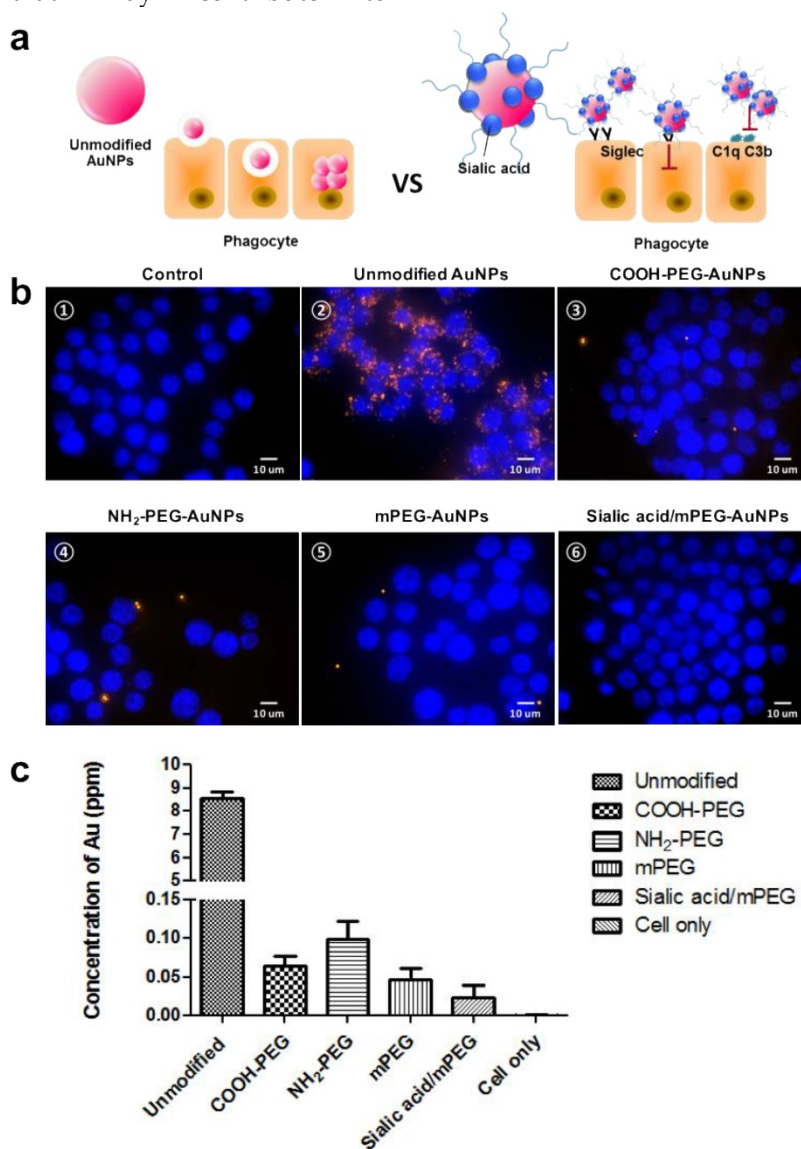


Figure 2. *In vitro* comparative analysis of cellular uptake after AuNP treatment. (a) Schematic illustration of cellular uptake of unmodified and sialic acid coated AuNPs. (b) Dark field images of cellular uptake of AuNPs after 24 h incubation in RAW264.7 cells ($15 \mu\text{g/mL}$): (b-①) Untreated control cells; (b-②) Unmodified AuNPs accumulated in the intracellular region; (AuNPs indicated by orange dots); (b-③-⑥) Various charged PEG AuNPs and sialic acid/mPEG AuNPs treated cells showed less uptake of AuNPs than unmodified AuNP treated cells, magnification ($60\times$), scale bar = $10 \mu\text{m}$. (c) ICP-MS analysis of AuNPs after $15 \mu\text{g/mL}$ AuNP treatment for 24 h in RAW264.7 cells. Data are means \pm SD ($n=5$).

Sialic acid-mediated suppression of immune response in macrophages

As the activation of macrophages increases phagocytosis, it is expected that the reduced cellular uptake of sialic acid/mPEG AuNPs would be attributed to the decreased immune response. Under optical microscopy, spindle-like morphology was observed in unmodified AuNP treated macrophages (Figure S5). However, the morphology of the macrophage with sialic acid/mPEG AuNPs was almost identical to that of untreated control, while those treated with PEG modified AuNPs exhibited spindle-like morphology. These results strongly encouraged us to investigate whether sialic acid is able to suppress the immune response of macrophages. Accordingly, mRNA level of representative activated macrophage markers, CD14 and CD86, was investigated using reverse transcript polymerase chain reaction (RT-PCR) (Figure 3). The

mRNA level of F4/80 was also evaluated as a general macrophage marker. The treatment of each type of AuNP showed negligible change in the mRNA level of F4/80, indicating that the inherent nature of macrophages remained unchanged. The unmodified AuNPs showed increased level of CD14 and CD86, whereas COOH-PEG AuNPs, mPEG AuNPs, and NH₂-PEG AuNPs exhibited similar levels of CD14 and slightly higher levels of CD86 compared to the untreated control. The reduced immune response of macrophages treated with PEG modified AuNPs was ascribed to the hydrating layers of PEG because these inhibit protein adsorption and clearance of nanoparticles *via* MPS [39]. In particular, for macrophages treated with sialic acid/mPEG AuNPs, mRNA levels of CD14 and CD86 were not only lower than those of PEG modified AuNP groups, but also similar to the untreated control.

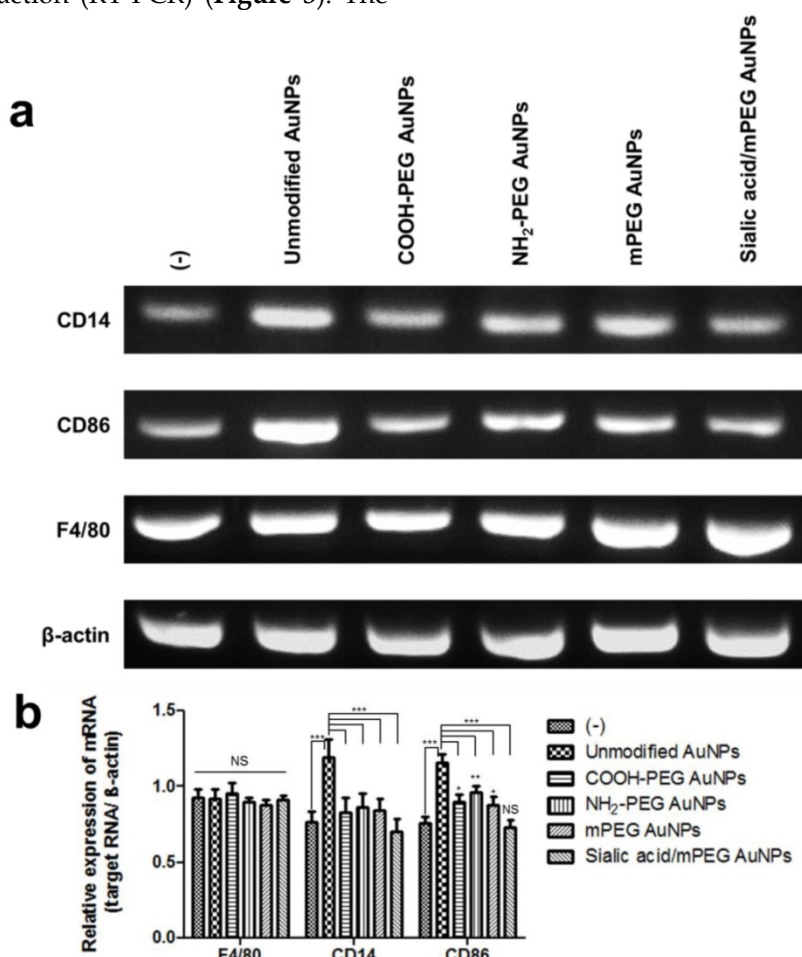


Figure 3. *In vitro* comparative analysis of CD14, CD86 and F4/80 mRNA expression after AuNPs treatment. (a) RT-PCR analysis of macrophage markers, CD14, CD86, and F4/80, mRNA expression levels in RAW264.7 cells after AuNP (15 µg/mL) treatment for 24 h: Representative images of three independent experiments (Lane 1: control group, no treatment; Lane 2: unmodified AuNPs treated group; Lane 3: COOH-PEG AuNPs treated group; Lane 4: NH₂-PEG AuNPs treated group; Lane 5: mPEG AuNPs treated group; Lane 6: sialic acid/mPEG AuNPs treated group). (b) Relative expression levels of mRNA in RAW264.7 cells after AuNP treatment for 24 h compared with that in untreated control group. Asterisks represent significant differences between cells treated with the corresponding different regimes (***p < 0.001, **p < 0.05, *p < 0.1; n = 3; one-way ANOVA with Newman-Keuls multiple comparison test). Data represent mean ± s.d. NS, not significant.

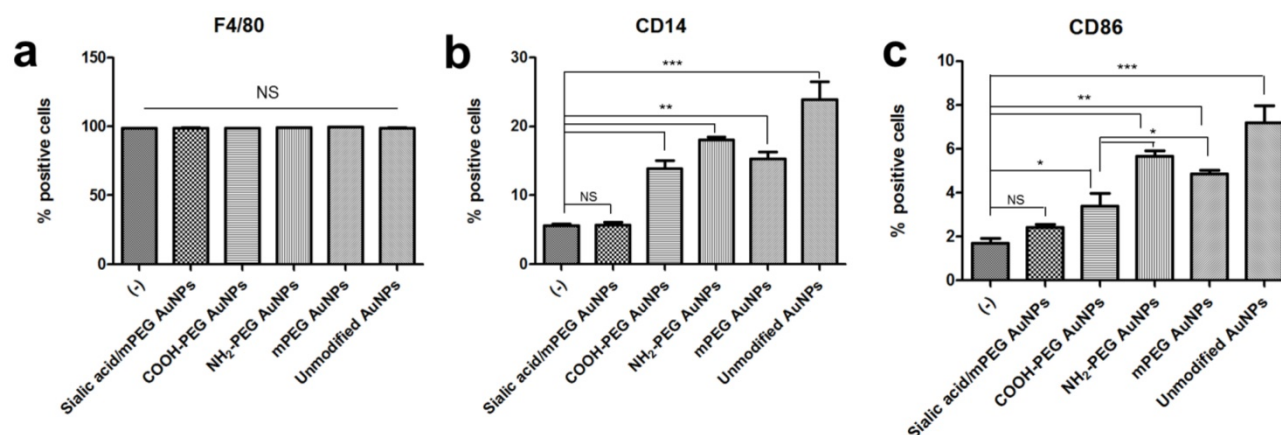


Figure 4. Comparative analysis of stimulated macrophage markers after AuNP treatment (a-c) Macrophage markers, F4/80, CD86, and CD14, expression levels were quantified by flow cytometry in RAW264.7 cells after AuNP (15 $\mu\text{g/mL}$) treatment for 24 h. Binding is expressed as median fluorescence intensity ($n = 3$ for all independent experiments). Asterisks represent significant differences between cells treated with the corresponding different regimes (** $p < 0.001$, * $p < 0.05$, $p < 0.1$; $n = 3$; one-way ANOVA with Newman-Keuls multiple comparison test). Data represent mean \pm s.d. NS, not significant.

The effects of sialic acid in the suppression of immune response were demonstrated in protein levels quantified by FACS analysis. In accordance with the RT-PCR results, F4/80 protein expression level remained constant after each AuNP treatment. PEG modification also decreased protein expression of CD14 and CD86 compared to the unmodified AuNPs, however, those levels were higher than untreated controls. Although PEG modified AuNPs with different charges showed negligible changes in CD14 and CD86 mRNA level, significant difference was observed in CD86 protein expression level. Negatively charged COOH-PEG AuNPs induced lower protein expression of CD86 than neutral mPEG AuNPs as well as positively charged NH₂-PEG AuNPs, while there was no significant difference in CD14 protein expression level among PEG modified AuNPs. These results imply that the negative charge has potential advantages in preventing the activation of macrophages *in vitro*. On the contrary, for macrophages treated with unmodified AuNPs and PEG modified AuNPs, there was no statistically significant difference in CD14 and CD86 protein expression levels between untreated and sialic acid/mPEG AuNPs treated macrophages.

The confocal microscopy images correlated well with the results observed by FACS (Figure 5 and Figure S6). PEG and sialic acid suppressed the expression of CD14 and CD86 which are markers for classically activated macrophages. However, it is noteworthy that the CD301 protein expression level remained unchanged after AuNP treatment. As CD301 is a marker for alternative macrophages [41], these results suggest that AuNPs did not induce macrophages to differentiate into M2 macrophages.

As activated macrophages secrete proinflammatory cytokines, the amounts of tumor

necrosis factor- α (TNF- α) and interleukin (IL)-6 were measured by enzyme-linked immunosorbent assay (ELISA). Secreted TNF- α levels, rated from highest to lowest, were observed in unmodified AuNPs, PEG modified AuNPs, sialic acid/mPEG AuNPs, and untreated macrophages (Figure 6a). In particular, TNF- α level was found to be 4.5 times lower in sialic acid/mPEG AuNPs than that in PEG modified AuNPs, indicating the immune suppressing effect of sialic acid. On the other hand, there is no statistical difference in IL-6 levels among macrophages with PEG modified AuNPs, sialic acid/mPEG AuNPs, and untreated macrophages, except that the one treated with unmodified AuNPs showed a higher level of secretion (Figure 6b). Taken together, these *in vitro* results suggest that in addition to the effects of PEG, sialic acid suppresses the immune stimulation of macrophages and subsequently enables the nanoparticles to evade phagocytosis.

Influence of sialic acid modification on *in vivo* accumulation

We envisaged that the ability of sialic acid to suppress the immune response and evade phagocytosis in macrophages would enhance the accumulation of nanoparticles in the tumor regions by evading RES organs including liver and spleen. In addition, sialic acid was expected to facilitate active targeting because it is well-known to bind lectins overexpressed in several tumors [32, 42, 43]. In order to validate the biodistribution of AuNPs *in vivo*, AuNPs were labeled with ⁶⁴Cu. In particular, the biodistribution study was expected to show the effects of sialic acid in active targeting as well as evasion of RES clearance since the EPR effect is presumed to be similar among all the tested AuNPs due to their similar hydrodynamic diameter.

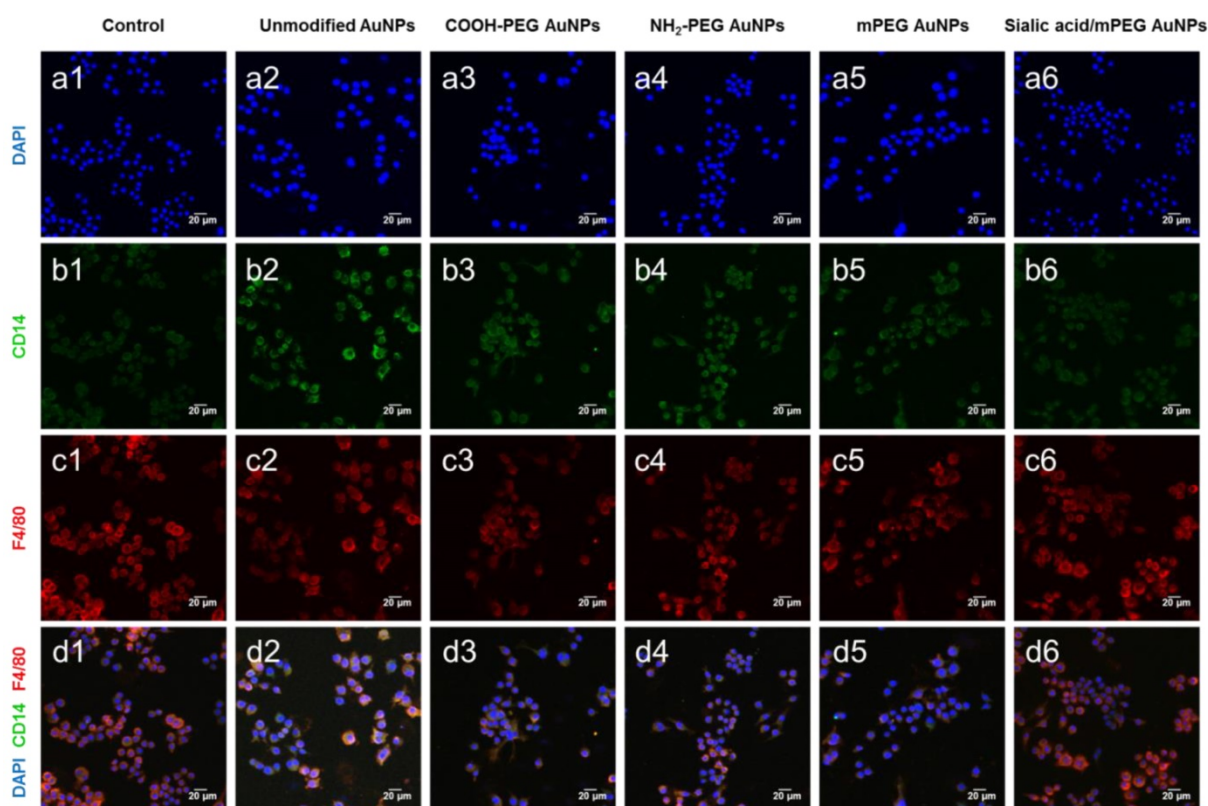


Figure 5. Representative confocal microscopy images of macrophage markers (CD14, F4/80) in RAW264.7 cells after AuNP treatment. Macrophage markers, CD14 and F4/80, were stained in RAW264.7 cells after AuNP (15 μg/mL) treatment for 24 h. (a) Nuclei are stained with DAPI (blue). (b) Classical activated macrophage surface marker, CD14 is observed as green fluorescence signal on the cell membrane surface. (c) Macrophage marker, F4/80 is observed as red fluorescence signal on the cell membrane surface. (d) Merged images of DAPI, CD14, and F4/80. Scale bar = 20 μm

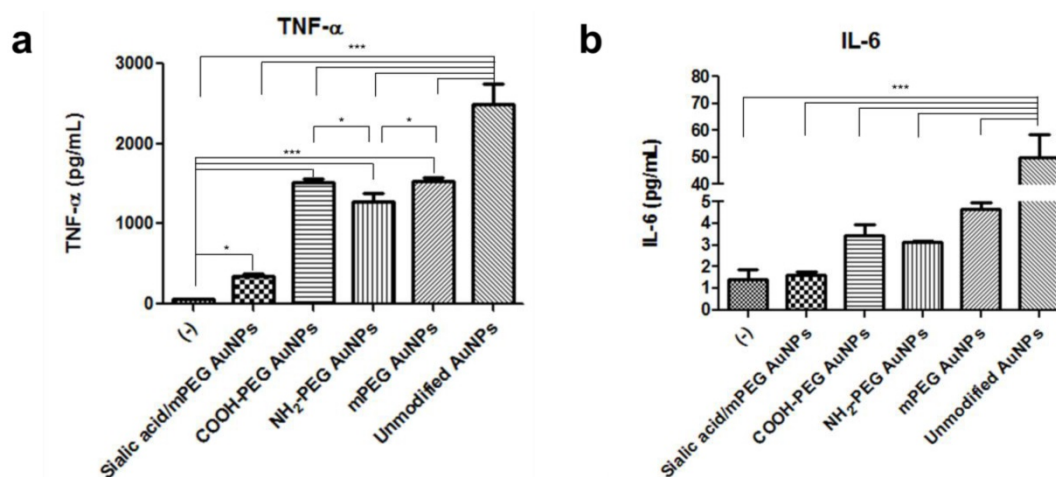


Figure 6. Comparative analysis of secreted proinflammatory cytokines after AuNP treatment (a) Proinflammatory cytokine, tumor necrosis factor-α (TNF-α), (b) interleukin (IL)-6 production was measured by ELISA in cell culture medium of the RAW264.7 cells after AuNP (15 μg/mL) treatment for 24 h, respectively. Asterisks represent significant differences between cells treated with the corresponding different regimes (**p < 0.001, *p < 0.05, *p < 0.1; n = 3; one-way ANOVA with Newman-Keuls multiple comparison test). Data represent mean ± s.d.

As shown in ITLC plate analysis, ⁶⁴Cu was successfully labeled onto each type of AuNP without any un-doped trace radiation (Figure S7). 4T1 tumor-bearing mice were prepared as 4T1 tumor overexpresses lectins which can bind to sialic acid [44]. ⁶⁴Cu-labeled AuNPs were injected intravenously to 4T1 tumor mice and the biodistribution was

evaluated at 1, 4, 24 and 48 h post-injection (Figure 7, Figure 8, and Figure S8). Unmodified AuNPs had high initial accumulation in spleen and liver, which dropped to similar levels as other AuNPs over time. It is of note that sialic acid/mPEG AuNPs showed almost twice as much tumor accumulation and half the spleen accumulation as compared to the other

AuNPs. In details, areas under curve (AUC) of spleen was found to be 2.0 and 1.5 times lower in sialic acid/mPEG AuNPs than in unmodified AuNPs and mPEG AuNPs respectively, indicating the immune suppressing effects of sialic acid. In addition, AUC of tumor showed 2.4 and 1.6 times higher in sialic acid/mPEG AuNPs than unmodified AuNPs and mPEG AuNPs respectively, implying sialic acid in enhanced accumulation of tumor (**Table S2**). These results suggest that sialic acid modification facilitates the evasion of RES clearance and subsequently promotes the enhancement of tumor accumulation, which is attributed to its ability to evade phagocytosis of macrophages by suppressing immune response. In addition, active targeting effects of sialic acid might contribute to the enhanced tumor accumulation of sialic acid/mPEG AuNPs in 4T1 tumor as well. Furthermore, treatment by sialic acid/mPEG AuNPs did not induce noticeable cytotoxicity (**Figure S9**), implying the potential application of surface

modification of sialic acid as a safe way to enhance tumor accumulation and evade the RES.

Conclusion

Herein, we investigated the ability of sialic acid in evading the immune response and prolonging the blood circulation of nanoparticles. *In vitro* macrophage studies demonstrated that sialic acid coating reduced cellular uptake of nanoparticles and suppressed immune response. *In vivo* quantitative pharmacokinetic studies confirmed that sialic acid modification enabled prolonged systemic circulation and improved tumor targeting ability of the nanoparticles. Taken together, sialic acid modification represents a new strategy of developing long-circulating nanocarriers with “self” markers, which is expected to advance the field of drug delivery and molecular imaging systems.

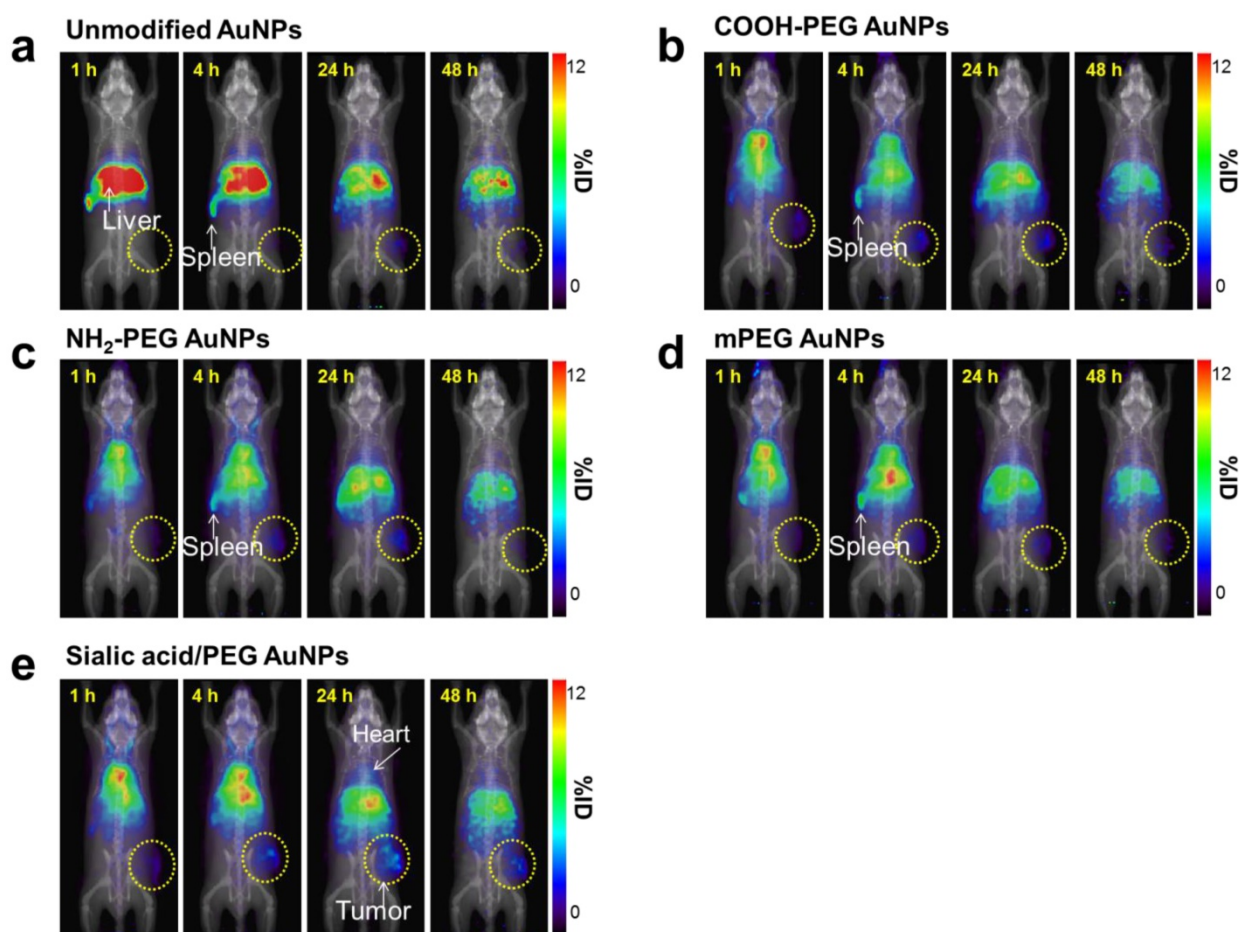


Figure 7. Whole-body PET images of ^{64}Cu -AuNPs at different time points (a-e) PET imaging of 4T1 tumor-bearing mice after i.v. injection of 1.85 MBq (50 μCi) of ^{64}Cu -unmodified AuNPs (a), ^{64}Cu -COOH-PEG AuNPs (b), ^{64}Cu - NH_2 -PEG AuNPs (c), ^{64}Cu -mPEG AuNPs (d), and ^{64}Cu -sialic acid/mPEG AuNPs (e) at 1, 4, 24, and 48 h, respectively. (n = 4/group).

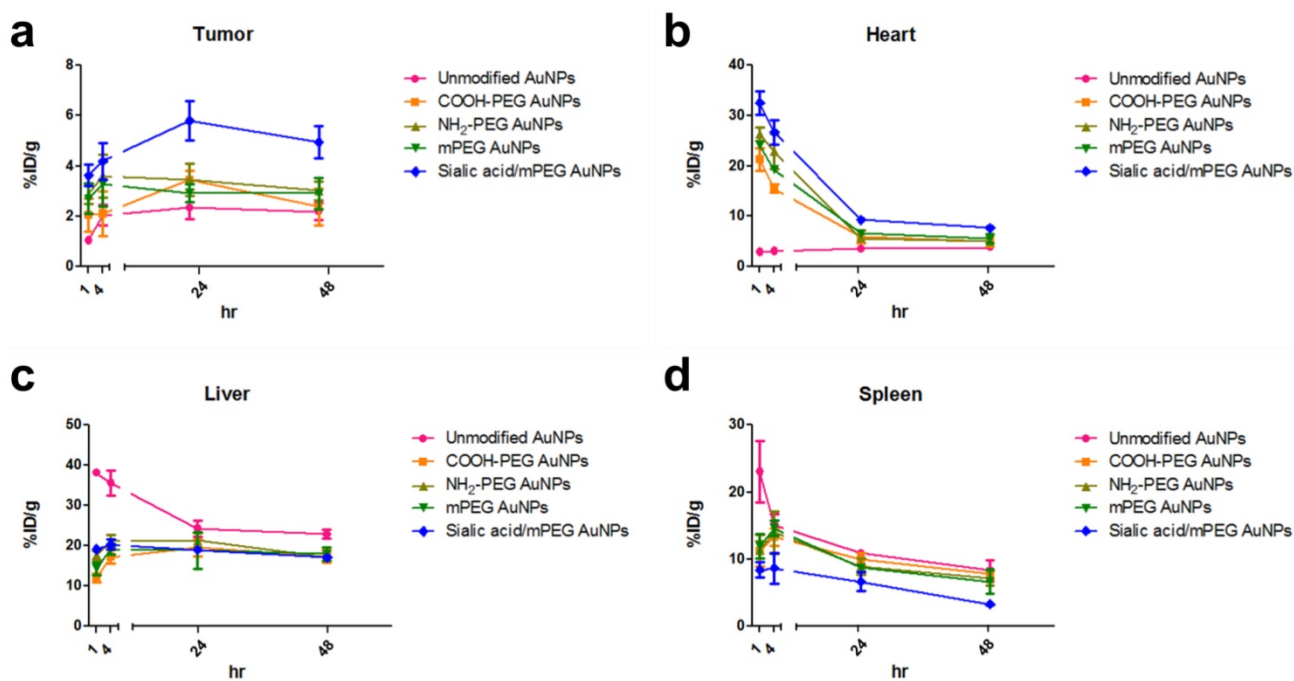


Figure 8. PET ROI Analysis of ^{64}Cu -AuNPs at different time points (a-d) The distribution of different AuNPs in tumor (a), heart (b), liver (c), and spleen (d) at 1, 4, 24, and 48 h after i.v. injection. The quantification is based on PET images ($n = 4/\text{group}$).

Supplementary Material

Supplementary figures and tables.

<http://www.thno.org/v07p0962s1.pdf>

Abbreviations

RES, reticuloendothelial system; PEG, polyethylene glycol; MPS, mononuclear phagocyte system; Siglec, sialic acid-binding immunoglobulin-like lectin; ITIM, intracellular immunoreceptor tyrosine-based inhibition motif; AuNPs, gold nanoparticle; ITLC, instant thin layer chromatography

Acknowledgments

This work was supported by a grant from the KRIBB Research Initiative Program (Korean Biomedical Scientist Fellowship Program), Korea Research Institute of Bioscience and Biotechnology, Republic of Korea, and the Intramural Research Program (IRP) of the National Institute of Biomedical Imaging and Bioengineering (NIBIB), National Institutes of Health (NIH). This research was also supported by the Global Innovative Research Center (GiRC) Program (2012K1A1A2A01055811) of the National Research Foundation of Korea.

Competing Interests

The authors have declared that no competing interest exists.

References

- Smith DM, Simon JK, Baker JR, Jr. Applications of nanotechnology for immunology. *Nat Rev Immunol.* 2013; 13: 592-605.
- Zolnik BS, Gonzalez-Fernandez A, Sadrieh N, Dobrovolskaia MA. Nanoparticles and the immune system. *Endocrinology.* 2010; 151: 458-65.
- Fang RH, Zhang L. Nanoparticle-Based Modulation of the Immune System. *Annu Rev Chem Biomol Eng.* 2016; 7: 305-26.
- Dobrovolskaia MA, McNeil SE. Immunological properties of engineered nanomaterials. *Nat Nanotechnol.* 2007; 2: 469-78.
- Li SD, Huang L. Nanoparticles evading the reticuloendothelial system: role of the supported bilayer. *Biochim Biophys Acta.* 2009; 1788: 2259-66.
- Blanco P, Shen H, Ferrari M. Principles of nanoparticle design for overcoming biological barriers to drug delivery. *Nat Biotechnol.* 2015; 33: 941-51.
- Jokerst JV, Lobovkina T, Zare RN, Gambhir SS. Nanoparticle PEGylation for imaging and therapy. *Nanomedicine (Lond).* 2011; 6: 715-28.
- Knop K, Hooogenboom R, Fischer D, Schubert US. Poly(ethylene glycol) in drug delivery: pros and cons as well as potential alternatives. *Angew Chem Int Ed Engl.* 2010; 49: 6288-308.
- Otsuka H, Nagasaki Y, Kataoka K. PEGylated nanoparticles for biological and pharmaceutical applications. *Adv Drug Deliv Rev.* 2003; 55: 403-19.
- Zhang P, Sun F, Liu S, Jiang S. Anti-PEG antibodies in the clinic: Current issues and beyond PEGylation. *J Control Release.* 2016; 244(Pt B): 184-93.
- Armstrong JK, Hempel G, Koling S, Chan LS, Fisher T, Meiselman HJ, et al. Antibody against poly(ethylene glycol) adversely affects PEG-asparaginase therapy in acute lymphoblastic leukemia patients. *Cancer.* 2007; 110: 103-11.
- Garay RP, El-Gewely R, Armstrong JK, Garratty G, Richette P. Antibodies against polyethylene glycol in healthy subjects and in patients treated with PEG-conjugated agents. *Expert Opin Drug Deliv.* 2012; 9: 1319-23.
- Longo N, Harding CO, Burton BK, Grange DK, Vockley J, Wasserstein M, et al. Single-dose, subcutaneous recombinant phenylalanine ammonia lyase conjugated with polyethylene glycol in adult patients with phenylketonuria: an open-label, multicentre, phase 1 dose-escalation trial. *Lancet.* 2014; 384: 37-44.
- Hong RL, Huang CJ, Tseng YL, Pang VF, Chen ST, Liu JJ, et al. Direct comparison of liposomal doxorubicin with or without polyethylene glycol coating in C-26 tumor-bearing mice: is surface coating with polyethylene glycol beneficial? *Clin Cancer Res.* 1999; 5: 3645-52.
- Holland JW, Hui C, Cullis PR, Madden TD. Poly(ethylene glycol)-lipid conjugates regulate the calcium-induced fusion of liposomes composed of phosphatidylethanolamine and phosphatidylserine. *Biochemistry.* 1996; 35: 2618-24.
- Varki A, Gagneux P. Multifarious roles of sialic acids in immunity. *Ann N Y Acad Sci.* 2012; 1253: 16-36.
- Munday J, Floyd H, Crocker PR. Sialic acid binding receptors (siglecs) expressed by macrophages. *J Leukoc Biol.* 1999; 66: 705-11.

18. Fearon DT. Regulation by membrane sialic acid of beta1H-dependent decay-dissociation of amplification C3 convertase of the alternative complement pathway. *Proc Natl Acad Sci U S A*. 1978; 75: 1971-5.
19. Kajander T, Lehtinen MJ, Hyvarinen S, Bhattacharjee A, Leung E, Isenman DE, et al. Dual interaction of factor H with C3d and glycosaminoglycans in host-nonhost discrimination by complement. *Proc Natl Acad Sci U S A*. 2011; 108: 2897-902.
20. Meri S, Pangburn MK. Discrimination between activators and nonactivators of the alternative pathway of complement: regulation via a sialic acid/polyanion binding site on factor H. *Proc Natl Acad Sci U S A*. 1990; 87: 3982-6.
21. Ram S, Sharma AK, Simpson SD, Gulati S, McQuillen DP, Pangburn MK, et al. A novel sialic acid binding site on factor H mediates serum resistance of sialylated *Neisseria gonorrhoeae*. *J Exp Med*. 1998; 187: 743-52.
22. Ferreira VP, Pangburn MK, Cortes C. Complement control protein factor H: the good, the bad, and the inadequate. *Mol Immunol*. 2010; 47: 2187-97.
23. Yu Z, Maoui M, Wu L, Banville D, Shen S. mSiglec-E, a novel mouse CD33-related siglec (sialic acid-binding immunoglobulin-like lectin) that recruits Src homology 2 (SH2)-domain-containing protein tyrosine phosphatases SHP-1 and SHP-2. *Biochem J*. 2001; 353: 483-92.
24. Whitney G, Wang S, Chang H, Cheng KY, Lu P, Zhou XD, et al. A new siglec family member, siglec-10, is expressed in cells of the immune system and has signaling properties similar to CD33. *Eur J Biochem*. 2001; 268: 6083-96.
25. Taylor VC, Buckley CD, Douglas M, Cody AJ, Simmons DL, Freeman SD. The myeloid-specific sialic acid-binding receptor, CD33, associates with the protein-tyrosine phosphatases, SHP-1 and SHP-2. *J Biol Chem*. 1999; 274: 11505-12.
26. Higuchi H, Shoji T, Murase Y, Iijima S, Nishijima K-i. Siglec-9 modulated IL-4 responses in the macrophage cell line RAW264. *Biosci Biotechnol Biochem*. 2016; 80: 501-9.
27. Wu Y, Lan C, Ren D, Chen G-Y. Induction of Siglec-1 by endotoxin tolerance suppresses the innate immune response by promoting TGF- β 1 production. *J Biol Chem*. 2016; 291: 12370-82.
28. Cho J, Kushiro K, Teramura Y, Takai M. Lectin-tagged fluorescent polymeric nanoparticles for targeting of sialic acid on living cells. *Biomacromolecules*. 2014; 15: 2012-8.
29. Spence S, Greene MK, Fay F, Hams E, Saunders SP, Hamid U, et al. Targeting Siglecs with a sialic acid-decorated nanoparticle abrogates inflammation. *Sci Transl Med*. 2015; 7: 303ra140.
30. Wang S, Yin D, Wang W, Shen X, Zhu JJ, Chen HY, et al. Targeting and Imaging of Cancer Cells via Monosaccharide-Imprinted Fluorescent Nanoparticles. *Sci Rep*. 2016; 6: 22757.
31. Bull C, Heise T, Adema GJ, Boltje TJ. Sialic Acid Mimetics to Target the Sialic Acid-Siglec Axis. *Trends Biochem Sci*. 2016; 41: 519-31.
32. Bondioli L, Ruozi B, Belletti D, Forni F, Vandelli MA, Tosi G. Sialic acid as a potential approach for the protection and targeting of nanocarriers. *Expert Opin Drug Deliv*. 2011; 8: 921-37.
33. Ghosh P, Han G, De M, Kim CK, Rotello VM. Gold nanoparticles in delivery applications. *Adv Drug Deliv Rev*. 2008; 60: 1307-15.
34. Kim CK, Ghosh P, Rotello VM. Multimodal drug delivery using gold nanoparticles. *Nanoscale*. 2009; 1: 61-7.
35. Kim YH, Jeon J, Hong SH, Rhim WK, Lee YS, Youn H, et al. Tumor targeting and imaging using cyclic RGD-PEGylated gold nanoparticle probes with directly conjugated iodine-125. *Small*. 2011; 7: 2052-60.
36. Templeton AC, Wuelfing WP, Murray RW. Monolayer-protected cluster molecules. *Acc Chem Res*. 2000; 33: 27-36.
37. Isecke R, Brossmer R. Synthesis of N-acetyl-9-S-acetyl-9-thioneuraminic acid, N-acetyl-9-thioneuraminic acid, and their methyl α -glycosides. *Carbohydr Res*. 1995; 274: 303-11.
38. Zheng JS, Zheng SY, Zhang YB, Yu B, Zheng W, Yang F, et al. Sialic acid surface decoration enhances cellular uptake and apoptosis-inducing activity of selenium nanoparticles. *Colloids Surf B Biointerfaces*. 2011; 83: 183-7.
39. Chithrani BD, Ghazani AA, Chan WC. Determining the size and shape dependence of gold nanoparticle uptake into mammalian cells. *Nano Lett*. 2006; 6: 662-8.
40. Salmaso S, Caliceti P. Stealth properties to improve therapeutic efficacy of drug nanocarriers. *J Drug Deliv*. 2013; 2013: 374252.
41. Solinas G, Schiarea S, Liguori M, Fabbri M, Pesce S, Zammataro L, et al. Tumor-conditioned macrophages secrete migration-stimulating factor: a new marker for M2-polarization, influencing tumor cell motility. *J Immunol*. 2010; 185: 642-52.
42. Jayant S, Khandare JJ, Wang Y, Singh AP, Vorsa N, Minko T. Targeted sialic acid-doxorubicin prodrugs for intracellular delivery and cancer treatment. *Pharm Res*. 2007; 24: 2120-30.
43. Bondioli L, Costantino L, Ballestrazzi A, Lucchesi D, Boraschi D, Pellati F, et al. PLGA nanoparticles surface decorated with the sialic acid, N-acetylneuraminic acid. *Biomaterials*. 2010; 31: 3395-403.
44. Monzavi-Karbassi B, Stanley JS, Hennings L, Jousheghany F, Artaud C, Shaaf S, et al. Chondroitin sulfate glycosaminoglycans as major P-selectin ligands on metastatic breast cancer cell lines. *Int J Cancer*. 2007; 120: 1179-91.